ADVANCED FUNCTIONAL MATERIALS

Supporting Information

for *Adv. Funct. Mater.,* DOI: 10.1002/adfm.202101792

Ligand and Anion Co-Leaching Induced Complete Reconstruction of Polyoxomolybdate-Organic Complex Oxygen-Evolving Pre-Catalysts

*Xiong Liu, Fanjie Xia, Ruiting Guo, Meng Huang, Jiashen Meng, Jinsong Wu, and Liqiang Mai**

Supporting Information

Ligand and Anion Co-Leaching Induced Complete Reconstruction of Polyoxomolybdate-Organic Complex Oxygen-Evolving Pre-Catalysts

*Xiong Liu, Fanjie Xia, Ruiting Guo, Meng Huang, Jiashen Meng, Jinsong Wu, and Liqiang Mai**

X. Liu, F. Xia, R. Guo, M. Huang, Dr. J. Meng, Prof. J. Wu, Prof. L. Mai, State Key Laboratory of Advanced Technology for Materials Synthesis and Processing, Wuhan University of Technology, Wuhan 430070, China
Prof. L. Mai, Foshan Xianhu Laboratory of the Advanced Energy Science and Technology Guangdong Laboratory, Xianhu hydrogen Valley, Foshan 528200, China

E-mail: mlq518@whut.edu.cn

Experimental section

1.1 Synthesis of Fe_xNi-POMo catalysts.

Its synthesis method refered to our previous work,[1] and the carbon substrate was simply replaced with nickel foam of the same size. In a typical synthesis of Ni-POMo catalyst, $(NH_4)_6Mo_7O_{24}\cdot 4H_2O$ (0.6 g), $Ni(NO_3)_2\cdot 6H_2O$ (0.4 g), 2-Methylimidazole (1 g) were added in methanol (70 mL). After stirring, the mixture and a piece of nickel foam (4 cm × 3 cm) was transfered into 100 mL Teflon-lined stainless-steel autoclave. After reaction at 160 °C for 20 h, the powder and nickel foam samples were washed with ethanol and dried for overnight. For the synthesis of Fe_xNi-POMo (x = 0.036, 0.052, 0.094), different molar ratios of Fe/Ni nitrate salts (5:1, 4:2, 3:3) were added, respectively. For the synthesis of Fe-POMo, the $Ni(NO_3)_2\cdot 6H_2O$ was replaced with $Fe(NO_3)_3\cdot 9H_2O$. Noted that the total number of moles of Ni/Fe salts remained consistent during the synthesis of each sample.

1.2 Characterizations.

Scanning electron microscopy (SEM) images and energy dispersive X-ray spectroscopy (EDS) were collected using a JEOL-7100F microscope at an acceleration voltage of 15 kV. Microscopy images, selected area electron diffraction (SAED) patterns, and elemental mappings were collected on JEM-2100F and Thermo Fisher Scientific Titan G260-300 scanning/transmission electron microscopes. X-ray photoelectron spectroscopy (XPS) and inductively coupled plasma atomic emission spectrometry (ICP-AES) measurements were carried out using an ESCALAB 250Xi instrument and PerkinElmer Optima 4300DV spectrometer, respectively. In/ex situ Raman spectra were recorded using a HORIBA HR EVO Raman system with an excitation wavelength of 633 nm. The temperature of solution was measured by a digital thermometer.

1.3 Electrochemical measurements.

All electrochemical measurements were carried out in a standard three-electrode setup which was connected to an electrochemical workstation (CHI760E). The nickel foam samples, Hg/HgO electrode, and graphite rod were used as working electrode, reference electrode, and counter electrode, respectively. There were two kinds of test conditions, one was 1 M KOH solution at room temperature, and the other was 30 wt.% KOH solution at 60.9 °C. For each kind of present data, the test conditions were indicated. All potentials for CV and LSV surves were converted to the RHE scale and iR-corrected by the resistance of electrolyte.

In situ electrochemistry-Raman tests were carried out using a HORIBA HR EVO Raman system (633 nm laser) and an electrochemical workstation of CHI760E. The new Hg/HgO and carbon rod were employed as the reference and counter electrodes, respectively. The $Fe_{0.052}$Ni-POMo arrays on the nickel foam directly served as working electrode. The LSV was tested at a scan rate of 0.2 mV s^{-1} in 1 M KOH at room temperature. Meanwhile, the Raman spectra were recorded with a potential interval of 30 mV.

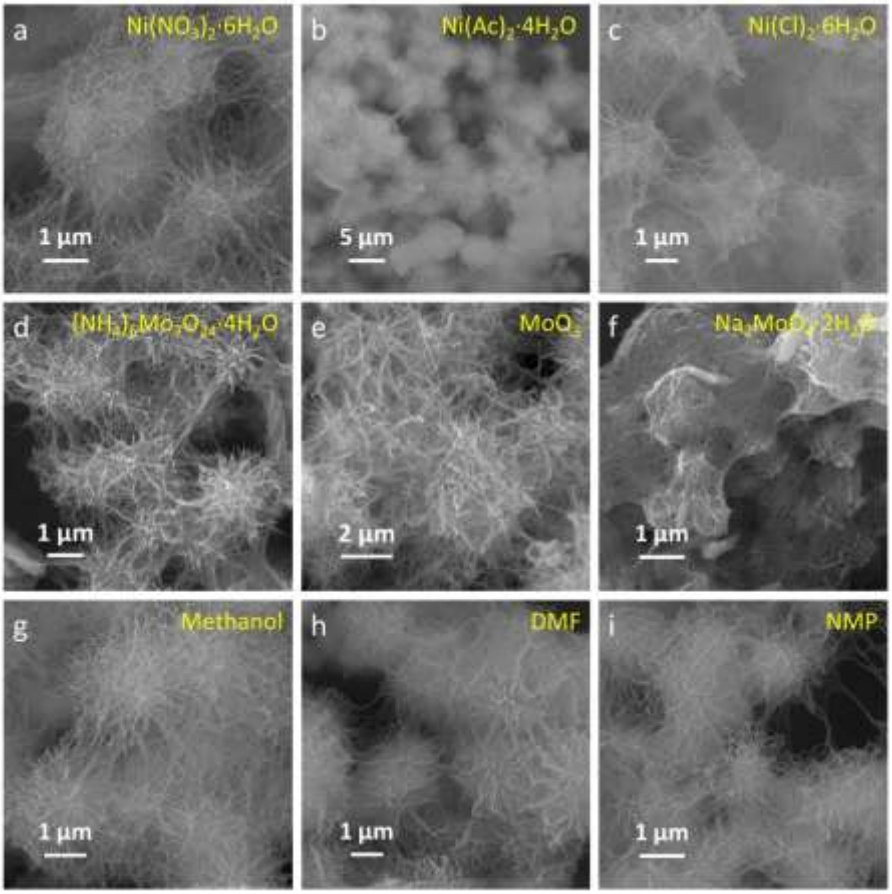

Figure S1. Morphology characterizations using different Ni/Mo-based sources or solvents as a single variable. a-c) SEM images of powders using different Ni-based sources. d-f) SEM images of powders using different Mo-based sources. g-i) SEM images of powders using different solvents.

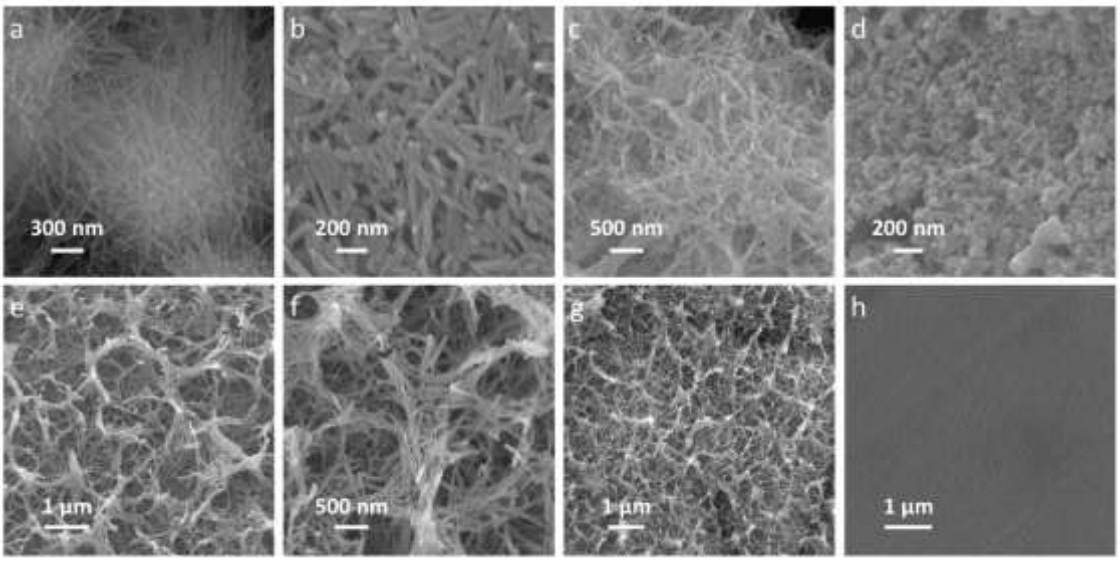

Figure S2. a-d) SEM images of Fe_xNi-POMo (x = 0, 0.036, 0.052, 0.094) powders. e-h) SEM images of Fe_xNi-POMo (x = 0, 0.036, 0.052, 0.094) grown on the nickel foam.

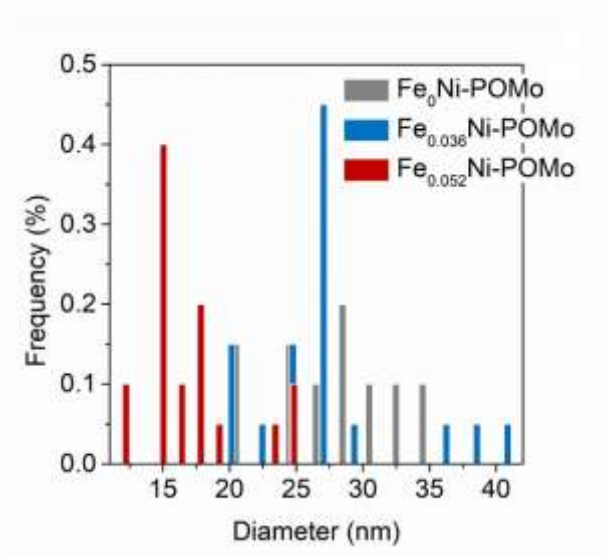

Figure S3. Size distributions of Fe_xNi-POMo (x = 0, 0.036, 0.052) nanowires measured on the HADDF-STEM images in Figure 2b-d.

In detail, the measured diameters of Fe_0Ni-POMo, $Fe_{0.036}Ni$-POMo, and $Fe_{0.052}Ni$-POMo nanowires range from 17.0 to 35.0 nm, from 20.2 to 40.9 nm, from 11.7 to 24.3 nm, respectively.

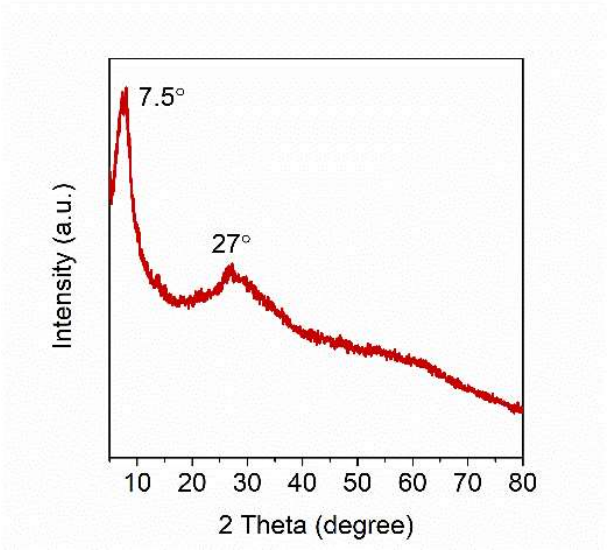

Figure S4. XRD pattern of $Fe_{0.052}Ni$-POMo powders.

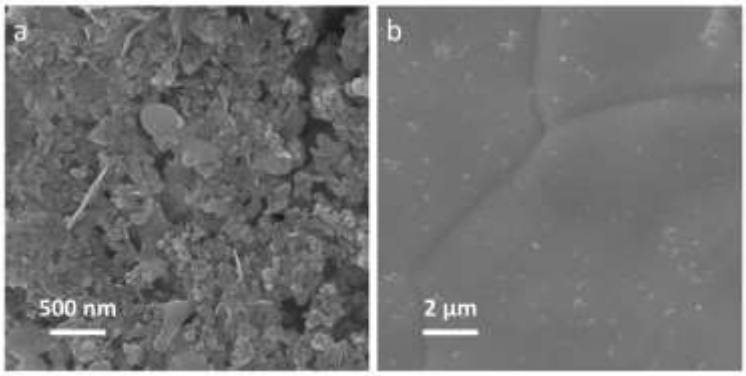

Figure S5. a,b) SEM images of Fe-POMo powders and nickel foam sample, respectively.

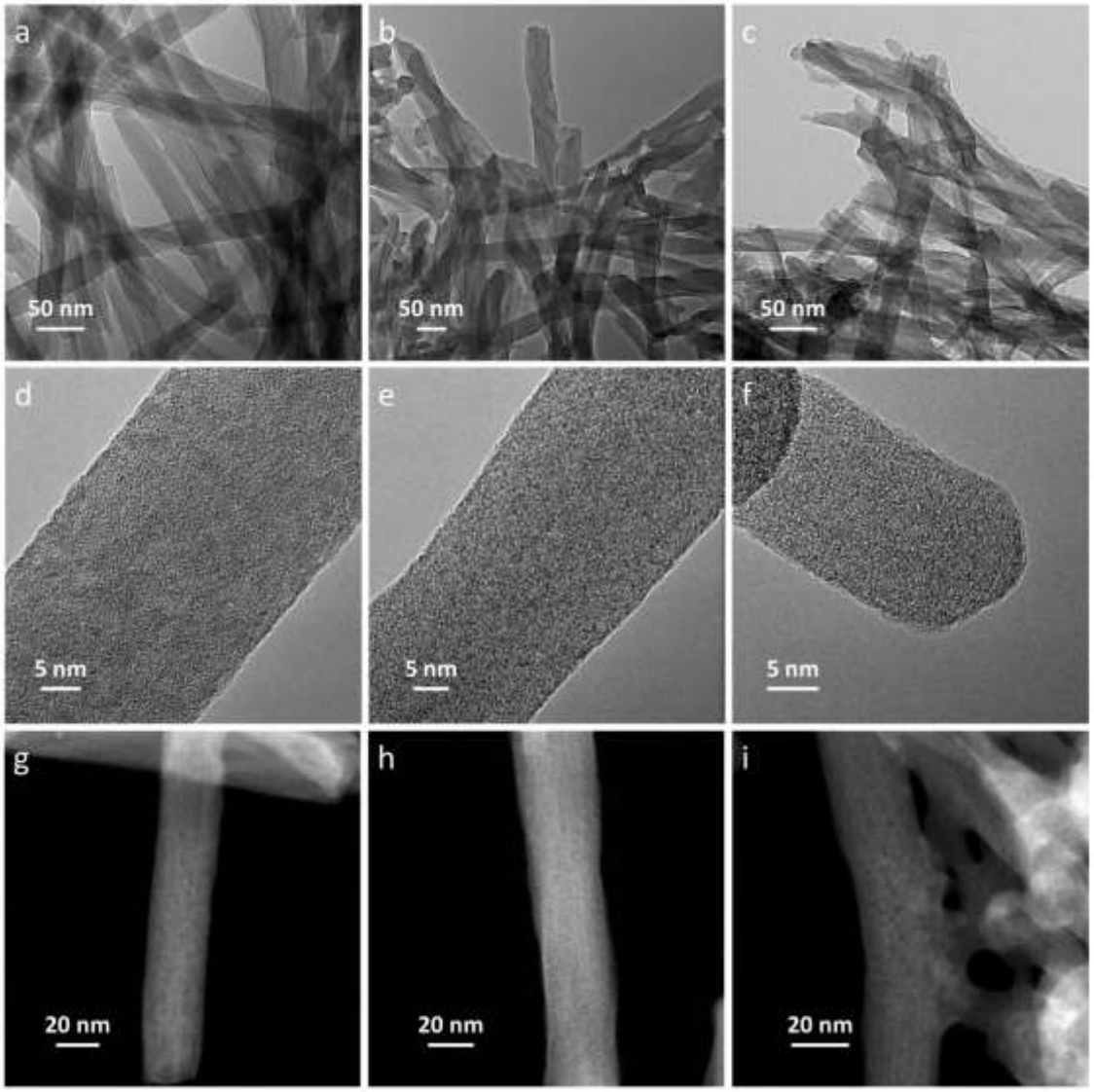

Figure S6. a-c) TEM images of Fe_xNi-POMo (x = 0, 0.036, 0.052) nanowires and their corresponding d-f) HRTEM and g-i) HAADF-STEM images.

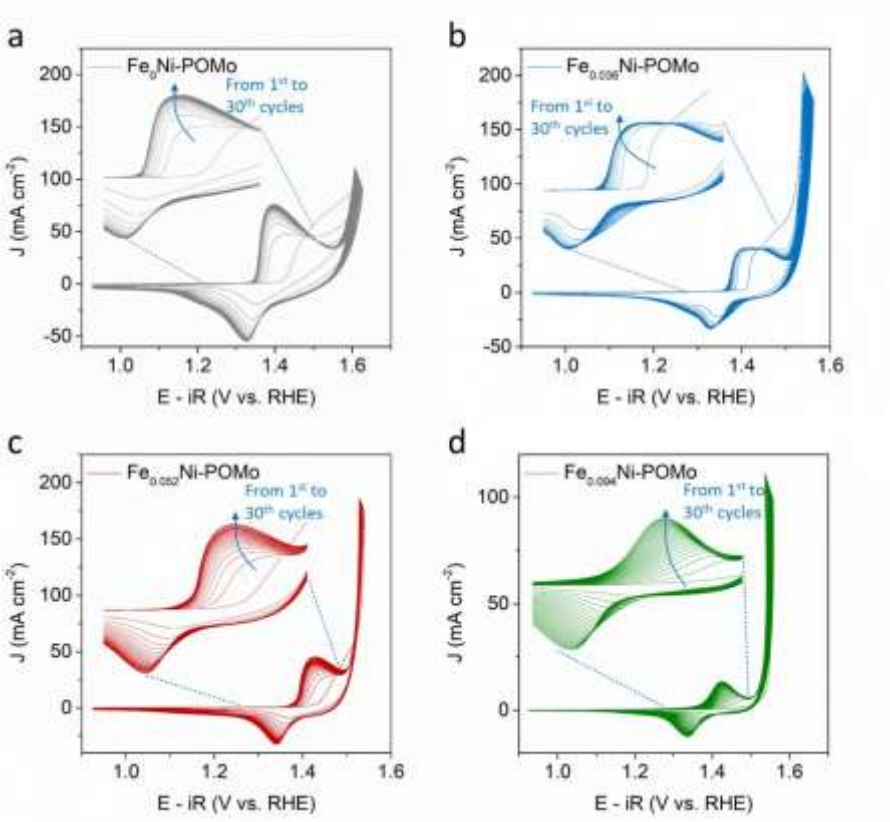

Figure S7. OER activation in 1 M KOH at room temperature. a-d) The initial 30-cycle CV curves of Fe_xNi-POMo (x = 0, 0.036, 0.052, 0.094) in 0-0.8 V vs. Hg/HgO at 50 mV s^{-1}, respectively.

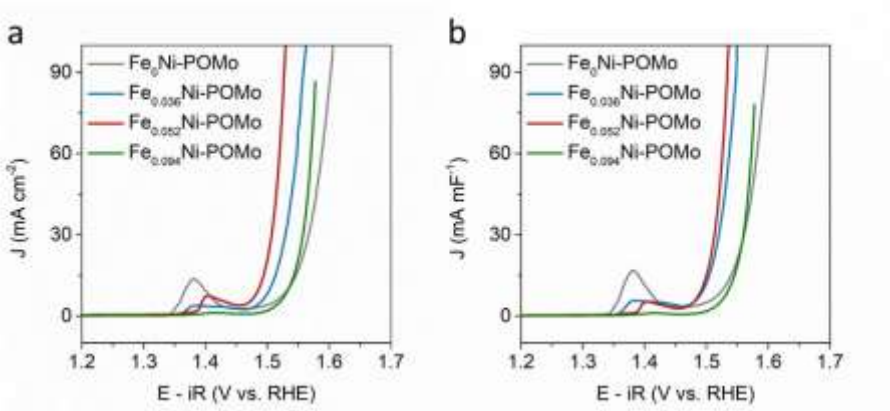

Figure S8. OER activity in 1 M KOH at room temperature. LSV curves of Fe_xNi-POMo normalized by (a) geometric area and (b) ECSA, respectively.

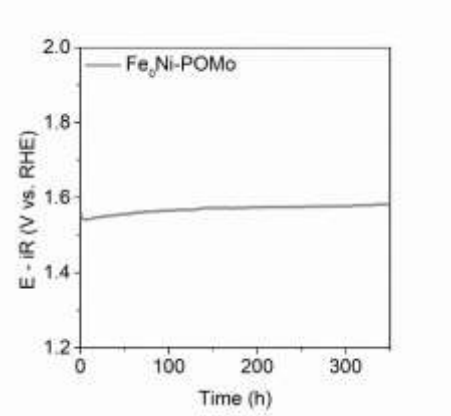

Figure S9. Chronopotentiometric curve of Fe_0Ni-POMo at 10 mA cm^{-2} in 1 M KOH at room temperature.

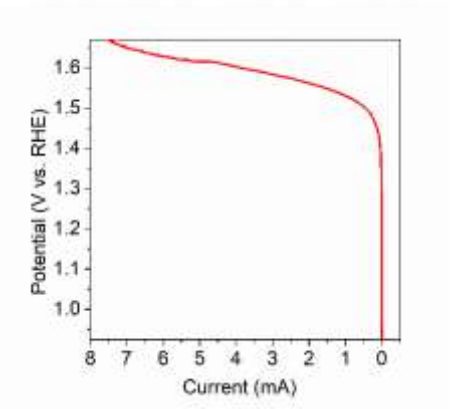

Figure S10. The recorded LSV curves during in situ Raman test at a scan rate of 0.2 mV s^{-1}.

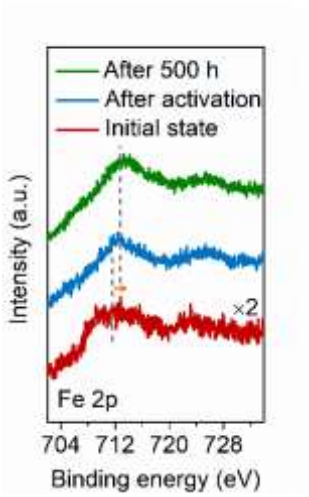

Figure S11. Fe 2p XPS spectra of $Fe_{0.052}$Ni-POMo initially, after CV activation, and after OER for 500 h.

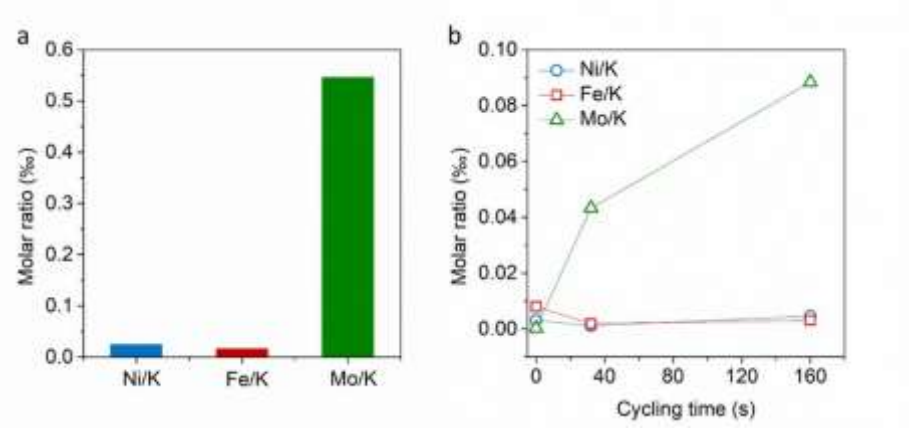

Figure S12. a) Molar ratios of Ni/K, Fe/K, and Mo/K in solution after soaking $Fe_{0.052}$Ni-POMo arrays in 1 M KOH for 32 s. b) Molar ratios of Ni/K, Fe/K, and Mo/K in solution after different CV cycle time of $Fe_{0.052}$Ni-POMo arrays in 1 M KOH.

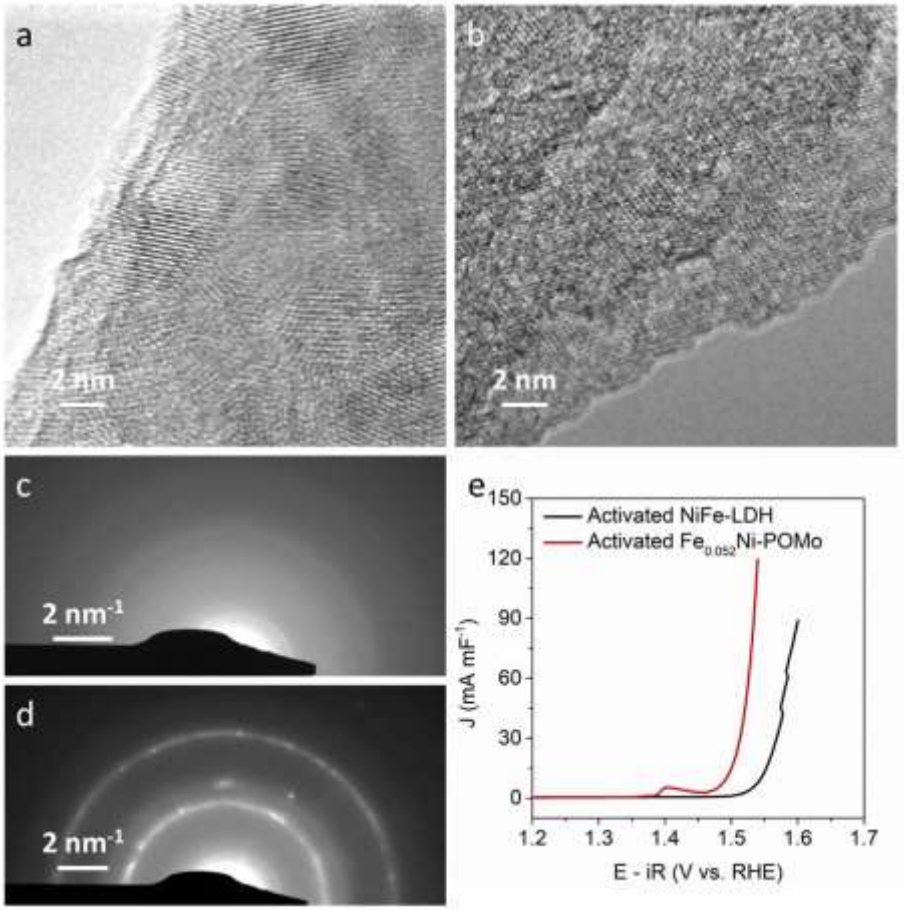

Figure S13. a,b) HRTEM images of activated $Fe_{0.052}$Ni-POMo and NiFe-LDH after 30-cycle CV tested in the potential range of 0-0.8 V vs. Hg/HgO in 1 M KOH, respectively. c,d) SAED patterns of activated $Fe_{0.052}$Ni-POMo and NiFe-LDH, respectively. e) ECSA-normalized LSV curves.

Table S1. Semiquantitative SEM-EDS elemental analysis of MoNi-2-mim powders using different nickel salts, molybdenum-based compounds or different solvents.

Raw materials		Mo molar content (%)	Ni molar content (%)
Ni sources	$Ni(NO_3)_2 \cdot 6H_2O$	56.54	43.46
	$NiCl_2 \cdot 6H_2O$	56.29	43.71
	$Ni(Ac)_2 \cdot 4H_2O$	57.07	42.93
Mo sources	$(NH_4)_6Mo_7O_{24} \cdot 4H_2O$	57.60	42.40
	MoO_3	59.79	40.21
	$NaMoO_4 \cdot 2H_2O$	56.85	43.15
Solvents	Methanol	56.54	43.46
	N,N-Dimethylformamide	56.36	43.64
	N-Methyl pyrrolidone	57.07	42.93

Table S2. Summary of OER performance for $Fe_{0.052}$Ni-POMo in this work and other reported POM catalysts or their derivates.

Catalysts	Testing conditions	OER activity	Tafel slope (mV dec^{-1})	Stability (h)	References
$Fe_{0.052}$Ni-POMo on the nickel foam	1 M KOH	255.3±1.6 mV at 10 mA cm^{-2}	43.8	545 h at 10 mA cm^{-2}	This work
Oxygenated-CoS_2-MoS_2 heteronanosheets (derived from $(NH_4)_4[M^{II}Mo_6O_{24}H_6] \cdot 6H_2O$ polyoxometalates)[2]	1 M KOH	272 mV at 10 mA cm^{-2}	45	10 h at 1.53 V_{RHE}	*ACS Catal.* **2018**, *8*, 4612
$[Co_{6.8}Ni_{1.2}W_{12}O_{42}(OH)_4(H_2O)_8]$ on the nickel foam[3]	0.1 M KOH (pH of 13)	360 mV at 10 mA cm^{-2}	126	10 h at 1.67 V_{RHE}	*Angew. Chem., Int. Ed.* **2017**, *56*, 4941
$Co_6Mo_6C_2$/NCRGO (derived from Co-doped polyoxometalate/conductive polymer/graphene oxide)[4]	1 M KOH	260 mV at 10 mA cm^{-2}	50	2000 CV cycles	*ACS Appl. Mater. Interfaces* **2017**, *9*, 16977
40% Ba[Co-POM][5]	1 M H_2SO_4	361 mV at 10 mA cm^{-2}	97	24 h at an overpotential of 250 mV	*Nat. Chem.* **2017**, *10*, 24
PW_{12}/Ag/graphene[6]	0.1 mol L^{-1} PBS (pH 7.0)	540 mV at 10 mA cm^{-2}	190	3 h at 1.84 V_{RHE}	*Eur. J. Inorg. Chem.* **2019**, *31*, 3597
Polyoxometalate intercalated NiFe LDHs[7]	O_2-bubbled 1 M KOH	287 mV at 10 mA cm^{-2}	43	40 h at 10 mA cm^{-2}	*Int. J. Hydrogen Energ* **2020**, *45*, 1802
Cu_6Co_7 POM on the carbon cloth[8]	Phosphate buffer (pH 7)	440 mV at 5 mA cm^{-2}; 500 mV at 10 mA cm^{-2}	147	~5 h at a fixed overpotential of 400 mV	*J. Mater. Chem. A* **2018**, *6*, 9915

References

[1] X. Liu, K. Ni, B. Wen, C. J. Niu, J. S. Meng, R. T. Guo, Q. Li, J. T. Li, Y. W. Zhu, X. J. Wu, D. Y. Zhao, L. Q. Mai, *J. Mater. Chem. A* **2018**, *6*, 17874.

[2] J. G. Hou, B. Zhang, Z. W. Li, S. Y. Cao, Y. Q. Sun, Y. Z. Wu, Z. M. Gao, L. C. Sun, *ACS Catal.* **2018**, *8*, 4612.

[3] W. J. Luo, J. Hu, H. L. Diao, B. Schwarz, C. Streb, Y.-F. Song, *Angew. Chem., Int. Ed.* **2017**, *56*, 4941.

[4] Y.-J. Tang, C.-H. Liu, W. Huang, X.-L. Wang, L.-Z. Dong, S.-L. Li, *ACS Appl. Mater. Interfaces* **2017**, *9*, 16977.

[5] M. Blasco-Ahicart, J. Soriano-López, J. J. Carbó, J. M. Poblet, J. R. Galan-Mascaros, *Nat. Chem.* **2017**, *10*, 24.

[6] Y. Li, X.-R. Chang, X.-J. Sang, J.-S. Li, Y.-H. Luo, Z.-M. Zhu, W.-S. You, *Eur. J. Inorg. Chem.* **2019**, *31*, 3597.

[7] X. Y. Xue, F. Yu, J.-G. Li, G. Bai, H. F. Yuan, J. Hou, B. H. Peng, L. Chen, M. Yuen, G. Wang, F. Wang, C. D. Wang, *Int. J. Hydrogen Energ* **2020**, *45*, 1802.

[8] M. Wang, W. Zhong, S. S. Zhang, R. J. Liu, J. M. Xing, G. J. Zhang, *J. Mater. Chem. A* **2018**, *6*, 9915.